



Environmental
Science
Nano

Leveraging Electrochemistry to Uncover the Role of Nitrogen in the Biological Reactivity of Nitrogen-Doped Graphene

Journal:	<i>Environmental Science: Nano</i>
Manuscript ID	EN-ART-07-2019-000802.R1
Article Type:	Paper
Date Submitted by the Author:	05-Sep-2019
Complete List of Authors:	Wang, Yan; University of Pittsburgh, Civil and Environmental Engineering Aquino de Carvalho, Nathalia; University of Pittsburgh, Civil and Environmental Engineering Tan, Susheng; University of Pittsburgh, Petersen Institute of Nanoscience and Engineering Gilbertson, Leanne; University of Pittsburgh, Civil and Environmental Engineering

SCHOLARONE™
Manuscripts

ENVIRONMENTAL SIGNIFICANCE STATEMENT

The ability to safely realize wide-ranging applications of graphene is limited by the inability to link properties that govern performance and that govern adverse impacts. Filling this gap will enable control of desired functional performance outcomes and adverse biological impacts through manipulations of graphene. Building on an established body of knowledge in graphene electrochemistry, the introduction of different N-bonding motifs is used to manipulate the electronic and bioactivity of N-doped graphene (NG). Key findings include, (i) similar trends between NG-mediated antioxidant oxidation and bacterial cytotoxicity suggesting a dominant oxidative stress mechanism and (ii) the correlation between the electrochemical oxygen reduction reaction and oxidative stress-related bioactivity demonstrating the important role of electron-donating graphitic-N in mediating bioactivity.

1
2
3
4
5
6
7
8
9
10
11
12
13
14
15
16
17
18
19
20
21
22
23
24
25
26
27
28
29
30
31
32
33
34
35
36
37
38
39
40
41
42
43
44
45
46
47
48
49
50
51
52
53
54
55
56
57
58
59
60

Leveraging Electrochemistry to Uncover the Role of Nitrogen in the Biological Reactivity of Nitrogen- Doped Graphene

Yan Wang¹, Nathalia Aquino de Carvalho¹, Susheng Tan², Leanne M. Gilbertson^{1,3}*

¹University of Pittsburgh, Department of Civil and Environmental Engineering, Pittsburgh,
Pennsylvania 15261, United States

²University of Pittsburgh, Department of Electrical and Computer Engineering, Swanson School
of Engineering and Petersen Institute of Nanoscience and Engineering, Pittsburgh, Pennsylvania
15261, United States

³University of Pittsburgh, Department of Chemical and Petroleum Engineering, Pittsburgh,
Pennsylvania 15261, United States

Revised for Submission to:

Environmental Science: Nano

September 9, 2019

*Corresponding Author: Phone: (412) 624-1683, e-mail: leanne.gilbertson@pitt.edu

ABSTRACT

While nitrogen doping greatly broadens graphene applications, relatively little is known about the influence of this heteroatom on the biological activity of graphene. A set of systematically modified nitrogen-doped graphene (NG) materials was synthesized using the hydrothermal method in which the degree of N-doping and N-bonding type is manipulated using two nitrogen precursors (urea and uric acid) and different thermal annealing temperatures. The bioactivity of the NG samples was evaluated using the oxidation of the intracellular antioxidant glutathione (GSH) and bacteria viability (of *Escherichia coli* K12), and oxidative stress was identified as the predominant antibacterial mechanism. Two key energy-relevant electrochemical reactions, oxygen reduction reaction (ORR) and oxygen evolution reaction (OER), were used to characterize the influence of different N-types on the electronic properties of the NG materials. Electron-donating graphitic-N and electron-withdrawing pyridinic-N were identified as effective promoters for ORR and OER, respectively. The similar mechanisms between the GSH oxidation (indicative of oxidative stress) and ORR mechanisms reveal the role of graphitic-N as the active site in oxidative stress related bioactivity, independent of other consequential properties (e.g., defect density, surface area). This work advances a growing rational design paradigm for graphene family materials using chemical composition and further provides valuable insight into the performance-hazard tradeoffs of NG applications in related fields.

INTRODUCTION

The one-atom-thick and high-aspect-ratio graphene gives rise to advantageous electronic, thermal, optical, and mechanical properties that enable diverse applications in energy storage and conversion, electronics, and biotechnology.¹⁻⁶ Research on biological interactions of graphene-based nanomaterials and the ability to manipulate properties to influence interactions at bio-interfaces are critical for not only understanding potential risks that graphene poses to environmental and human health through increased use, but also for enabling their biomedical and bioanalytical development.⁷⁻¹⁰ In addition, resolving the material properties that govern impacts of graphene-based nanomaterials at bio-interfaces is critical to developing rational design guidelines to meet desired functional performance outcomes in these applications while minimizing the potential for unintended consequences.¹¹

Chemical doping of graphene with heteroatoms, particularly nitrogen, is an effective approach to tailor electronic properties and chemical reactivity of graphene, which contributed to the emergence of (bio)electronic, (bio)sensor, electrocatalyst, and energy storage and conversion applications.¹²⁻¹⁷ However, to date, very little is known about the influence of nitrogen doping on the biological activity of graphene. The similarity in the atomic size of nitrogen and carbon, and the five available valence electrons enable relatively facile replacement of carbon with nitrogen in the graphene lattice by forming strong covalent bonds.¹⁴ Differences in electronegativity and electron density introduce charge redistribution between nitrogen dopants and adjacent carbon atoms. The resulting changes in spin density and charge distribution of these carbon atoms bring about more active sites on the graphene, accelerating electron transfer and improving the (electro)catalytic activity of graphene.^{12, 13, 18-20} While pure graphene is a zero-bandgap semimetal, nitrogen doping shifts the Fermi level and opens up the bandgap, enabling the

1
2
3 transformation of graphene to a *n*- or *p*-type semiconductor depending on the particular nitrogen
4 configurations.^{16, 21-23} Nitrogen doping is a facile doping process that effectively modulates the
5 structure and physicochemical properties of graphene while maintaining high electrical
6 conductivity.²⁴
7
8
9

10
11
12 Our previous study on reduced graphene oxide (rGO) demonstrates the positive correlation
13 between electrochemical activity and the propensity to induce biological oxidative stress.⁷
14 Decoupling these activities (e.g., by identifying another structural or property feature that
15 correlates independently with biological oxidative stress) would elucidate opportunities to design
16 graphene-family materials with enhanced electrochemical performance while reducing the
17 potential for adverse biological impacts. Previous findings of nitrogen-doped carbon
18 nanomaterials (carbon nanotubes, graphene, carbon dots) suggest the potential opportunity to
19 decouple the governing properties due to suggested biocompatibility.²⁵⁻³² On the other hand, in
20 our efforts to probe underlying mechanisms of electrochemical and biological reactions of
21 oxygen functionalized carbon nanomaterials,⁷⁻⁹ we identified electron transfer properties
22 common to both activities that are similarly tuned by different surface functional groups. In this
23 work, we investigate the potential for nitrogen doping to (i) decouple function and biological
24 reactivity of graphene, and (ii) establish the foundation for a new paradigm linking inherent
25 electronic and biological activities of carbon nanomaterials.
26
27
28
29
30
31
32
33
34
35
36
37
38
39
40
41
42
43

44
45 N-doped graphene (NG) contains four primary nitrogen configurations in the graphene lattice:
46 pyridinic-N, pyrrolic-N, graphitic-N, and N-oxide.^{13, 20, 33, 34} The nitrogen bonding
47 configurations, not the total nitrogen content, have been identified as the key factor for the
48 performance of important electrochemical reactions (e.g., oxygen reduction reaction (ORR) and
49 oxygen evolution reaction (OER)), with pyridinic-N or/and graphitic-N configurations
50
51
52
53
54
55
56
57
58
59
60

1
2
3 commonly considered as active catalytic sites.^{12, 13, 35-38} To further resolve the role of N in the
4 biological activity of NG and the potential to decouple from electrochemical activities, we
5 systematically prepared a set of NG materials with varying degrees of N-doping and different N-
6 types using a hydrothermal method. The degree of nitrogen doping and configurations of
7 nitrogen in doped graphene is tailored by using two different nitrogen precursors (urea and uric
8 acid) and thermal annealing under different temperatures. The bioactivity of the prepared
9 materials is evaluated as the inactivation of a bacterial model organism, *Escherichia coli* (*E. coli*)
10 K12, and the propensity to oxidize the intracellular antioxidant, glutathione (GSH). Two
11 important and well-studied electrochemical reactions, ORR and OER, are used (i) as
12 representative functional performance metrics (relevant to energy-related electrochemical
13 reactions), and (ii) to characterize the inherent electronic behavior of different NG materials as
14 the potential mechanism underlying different biological activities.
15
16
17
18
19
20
21
22
23
24
25
26
27
28
29
30

31 **MATERIALS AND METHODS**

32 **Chemicals and materials**

33
34
35
36 Single layer graphene oxide (GO) powder (~99% purity) prepared using Hummer's method
37 was purchased from ACS Materials LLC (Medford, MA, USA, product no. GNOP20A5), and
38 used as the starting material to synthesize N-doped graphene. Uric acid ($\geq 99\%$), methylene blue,
39 platinum (20% on carbon black), iridium (IV) oxide (IrO_2 , 99.99% metals basis), and Nafion
40 perfluorinated resin solution (5 wt% in mixture of lower aliphatic alcohols and water) were
41 obtained from Sigma-Aldrich (St. Louis, MO, USA). Urea ($\geq 99\%$), reduced glutathione (GSH),
42 bicarbonate (NaHCO_3), tris(hydroxymethyl) aminomethane (TRIS, 99.85%), hydrochloric acid
43 (HCl, 36.5 – 38%), Ellman's reagent (5,5'-dithio-bis-(2-nitrobenzoic acid), DTNB), dimethyl
44 sulfoxide (DMSO, $\geq 99.9\%$), potassium hydroxide (KOH, 85.8%), isopropanol (molecular
45
46
47
48
49
50
51
52
53
54
55
56
57
58
59
60

1
2
3 biology grade, $\geq 99.9\%$), sodium chloride (NaCl, 99.6%), Bacto agar, and Luria-Bertani (LB)
4
5 Lennox broth (Lot 163854) were obtained from Fisher Scientific (Pittsburgh, PA, USA).
6
7 Polypyrrole was purchased from Toronto Research Chemicals (Toronto, ON, Canada).
8
9 Deionized (DI) water was produced by Millipore Synergy UV Water Purification System and
10
11 used as solvent for all chemicals, unless otherwise specified.
12
13

14 **Synthesis of a systematic N-doped graphene material set**

15
16 300 mg of GO was dispersed in 200 mL of deionized water by bath sonication (VWR
17
18 Aquasonic 150T) for 1 h, and then mixed with urea in a 1: 30 mass ratio and with uric acid in a
19
20 1: 10 mass ratio, respectively. The mixture was stirred for 1 h and then sealed in a 300 mL
21
22 Teflon-lined autoclave and remained at 175°C for 12 h. After the autoclave was cooled down to
23
24 the room temperature, the solids were filtered and washed and finally dried by lyophilization.
25
26 The samples after this one-pot hydrothermal process are named as NG-U and NG-UA (i.e., N-
27
28 doped reduced GO (NG) with urea and uric acid as the nitrogen precursor), respectively. One
29
30 rGO sample was also prepared using the same experimental procedure but without addition of
31
32 the N precursor, which serves as the control for NG-U and NG-UA samples.
33
34
35

36
37 Further, two annealed samples were prepared for each N-precursor set. NG-U or NG-UA was
38
39 transferred to a tube furnace (Thermo Scientific Lindberg/Blue M TF55035A-1) and heated to
40
41 the target temperature at a heating rate of 5 °C min⁻¹ and annealed for 30 min under a helium gas
42
43 flow. The samples after annealing NG-U at 650 °C and 950 °C are denoted by NG-U-650 and
44
45 NG-U-950, respectively. The samples after annealing NG-UA at 650 °C and 800 °C are denoted
46
47 by NG-UA-650 and NG-UA-800, respectively.
48
49
50

51 **Material characterization**

1
2
3 N-doped graphene samples were characterized using X-ray photoelectron spectroscopy (XPS,
4 to determine the elemental composition and distribution of N-types through peak deconvolution
5 of N1s spectra), Raman spectroscopy (to determine defect density and the shift between *n*- and *p*-
6 doping), transmission electron microscopy (TEM, to evaluate the morphology and obtain the
7 mapping of elemental distribution), Brunauer-Emmett-Teller (BET) analysis (to measure the
8 surface area), and methylene blue adsorption (to evaluate the dispersed surface area in
9 suspension). The methodological details of these characterization techniques are described in the
10 Supporting Information (SI).
11
12
13
14
15
16
17
18
19
20

21 **Evaluation of biological activity**

22
23
24 *GSH oxidation by the NG samples.* GSH oxidation by the NG samples was evaluated
25 following the same procedure detailed in our previous publications.^{7-9, 39} Briefly, reduced GSH
26 (0.4 mM) was exposed to the NG samples (0.05 mg mL⁻¹, buffered at pH=8.6) and monitored for
27 6 h in the dark at room temperature under constant rotation. Measurements were performed at
28 different time points (0.25, 0.5, 1, 2.5, 4, and 6 h). At each time point, the suspension was passed
29 through a 0.22 µm syringe filter (MilliporeSigma) to remove the graphene sample. 0.9 mL of the
30 filtrate was then combined with 1.57 mL Tris-HCl buffer (pH=8.3) and 30 µL of Ellman's
31 reagent (0.1 M). The absorbance at 412 nm was measured using a UV-vis spectrophotometer and
32 then used to determine the concentration of non-oxidized GSH. The percent loss of GSH was
33 calculated compared to the control (no NG). Average and standard deviations were determined
34 from three replicates.
35
36
37
38
39
40
41
42
43
44
45
46
47
48

49 Kinetic rates of GSH oxidation were calculated following our previous studies.^{7, 39} Rapid
50 adsorption of reactant (i.e., GSH) and desorption of product (e.g. glutathione disulfide) from the
51
52
53
54
55
56
57
58
59
60

1
2
3 sample surface is assumed in the kinetic model. The interaction between GSH and the NG
4 samples is expressed with the following first-order rate law:
5
6

$$-\frac{d[\text{GSH}]}{dt} = k[\text{GSH}][\text{NG}] \rightarrow \ln[\text{GSH}] = -k[\text{NG}]t + C \quad (1)$$

7
8
9

10 where k is the rate constant ($\text{mL mg}^{-1} \text{h}^{-1}$), $[\text{GSH}]$ is the concentration of free GSH in solution,
11 $[\text{NG}]$ is the concentration of the NG sample (0.05 mg mL^{-1}), C is a constant of this integration
12 equation and denotes the natural logarithm of the initial GSH concentration.
13
14
15

16 *Antibacterial activity of the NG samples in suspension.* *E. coli* K12 (CGSC #7740, Yale Coli
17 Genetic Stock Center, New Haven, CT, USA) was used as a model Gram-negative bacterium to
18 evaluate antimicrobial activities of the NG samples. Cultures were grown overnight in LB
19 Lennox broth at 37°C and harvested at mid-exponential log phase. To remove residual growth-
20 medium constituents prior to exposure to the prepared NG samples, cell cultures were (i)
21 centrifuged at 10,000 rpm for 1 min to pellet cells, (ii) the supernatant was decanted and replaced
22 with saline solution (0.9% NaCl), and (iii) the cells were re-suspended in saline solution. This
23 washing step was repeated three times.
24
25
26
27
28
29
30
31
32
33
34
35

36 The NG samples (0.2 mg mL^{-1}) dispersed in saline solution were bath sonicated for 1 h before
37 being exposed to the bacteria. For the exposure, 3 mL of the sonicated NG samples was mixed
38 with 30 μL of bacteria solution ($\sim 10^7$ colony forming units (CFU) mL^{-1}) for 4 h at room
39 temperature under constant rotation. In addition to directly plating the suspension after 4 h
40 exposure, the bacteria suspension was bath sonicated for 10 min after the 4 h reaction release
41 viable bacteria that are wrapped by NG aggregates, as in previous studies.⁴⁰⁻⁴⁴ After both the
42 exposure period and the sonication step, bacteria inactivation was evaluated using a colony
43 counting method. Briefly, 100 μL of bacteria suspension was immediately plated on LB agar
44 plates and incubated for 17 h at 37°C for CFU enumeration. The percent inactivation was
45
46
47
48
49
50
51
52
53
54
55
56
57
58
59
60

1
2
3 calculated by comparing the exposure to the control (i.e., bacteria solution without the NG
4 samples). All treatments were prepared in triplicate and repeated in three independent
5 experiments. All materials and chemicals used for antimicrobial activity experiments were
6 sterile.
7
8
9
10

11
12 GraphPad Prism version 8.1.0 (La Jolla, California, USA) was used to assess the difference in
13 the GSH oxidation and the bacterial inactivation by rGO and NG samples. One-way ANOVA
14 with Tukey's multiple comparison test was used to compare three or more treatments at each
15 time point, and two-tailed *t*-test was used when there were only two treatments to compare.
16 Moreover, linear regression model was applied for GSH oxidation results and the slopes of
17 curves from different treatments were compared via the extra sum-of-squares F test. The
18 significance level is 95%, i.e., *P* values smaller than 0.05 are considered statistically significant.
19
20
21
22
23
24
25
26
27

28 **Electrochemical measurements**

29
30 For electrochemical characterization, the working electrodes were prepared as follows: (i) 2
31 mg of sample was mixed with 600 μL deionized water, 390 μL isopropanol, and 10 μL of
32 Nafion (5 wt%) followed by 15 min probe sonication (Branson S-450 digital ultrasonic
33 homogenizer) and 2 h bath sonication to form a well-dispersed suspension, (ii) 10 μL of the
34 dispersed mixture was carefully deposited on the glassy carbon disk electrode surface (0.1963
35 cm^2) and dried at room temperature for 2 h. The working electrodes were then tested in a three-
36 electrode cell with a platinum counter electrode and an Ag/AgCl reference electrode. The values
37 of potential are referenced against Ag/AgCl unless otherwise specified. Also, commercial noble
38 metal catalysts Pt/C and IrO₂ were used as reference materials for ORR and OER, respectively.
39
40
41
42
43
44
45
46
47
48
49
50

51 The ORR experiments by rotating ring-disk electrode (RRDE) voltammetry were carried out
52 using the same procedures described in our previous research.⁷ Briefly, 1 M KOH electrolyte
53
54
55
56
57
58
59
60

1
2
3 solution was used for all ORR experiments. Prior to each measurement, the electrolyte was
4 bubbled with N₂ for 30 min and the working electrode was cleaned by cyclic voltammetry for 25
5 cycles sweeping from 0.2 to -1 V. Next, the electrolyte was saturated with O₂ for 30 min before
6 performing RRDE tests. RRDE voltammetry was conducted from 0.2 to -1 V at a scan rate of 5
7 mV s⁻¹ with varying rotating speeds of 400, 625, 900, 1600, and 2500 rpm. The ring potential
8 was held at 0.5 V. The electron transfer number (*n*) and the percentage of H₂O₂ released during
9 ORR were determined using the following equations:

$$n = \frac{4I_D}{I_D + \frac{I_R}{N}} \quad (2)$$

22
23 and

$$\%H_2O_2 = 200 \times \frac{\frac{I_R}{N}}{I_D + \frac{I_R}{N}} \quad (3),$$

24
25
26
27
28
29 where *I_D* is the measured disk current (mA), *I_R* is the measured ring current (mA), and *N* is the
30 H₂O₂ collection coefficient at the ring (25.6%, provided by PINE Research Instrument). The
31 onset potentials of ORR polarization curves were determined from the intersection of the
32 tangents between the baseline and the rising reduction current.
33
34
35
36
37

38
39 The OER experiments using rotating disk electrode (RDE) were performed in 1 M KOH
40 electrolyte from 0 to 0.7 V with a scan rate of 5 mV s⁻¹ and a rotating speed of 1600 rpm. The
41 electrolyte was saturated with O₂ before the experiments and the O₂ flow was maintained over
42 the electrolyte during the measurements to ensure the O₂/H₂O equilibrium.
43
44
45
46
47

48 RESULTS AND DISCUSSION

49 Preparation and characterization of systematically modified N-doped graphene (NG)

50
51
52
53 *Changing nitrogen precursors and annealing temperatures effectively tunes the N-doping*
54 *states.* The hydrothermal method was used to synthesize NG samples because it is a facile and
55
56
57

1
2
3 eco-friendly method compared to other complex, low-yield, and costly techniques such as
4 chemical vapor deposition and nitrogen plasma process.^{14, 34, 35, 45, 46} The hydrothermal method
5
6 has also been shown to attain a higher level of nitrogen doping compared to other methods such
7
8 as thermal annealing, electrothermal reaction, and arc-discharge.^{13, 14, 46} In the hydrothermal
9
10 process, supercritical water acts as an alternative green reducing agent to organic solvents.
11
12 Nitrogen precursors are mixed with GO in a hydrothermal autoclave reactor, and nitrogen doping
13
14 occurs concomitantly with the elimination of oxygen groups on the GO. Given that nitrogen
15
16 precursors affect the nature of N-types in NG,⁴⁷ urea and uric acid were used as nitrogen sources
17
18 to introduce distinct properties and further different performance of samples between two
19
20 precursor NG sets. A comparison of two precursor NG sets is anticipated to identify the
21
22 governing material properties leading to more conclusive results.
23
24
25
26
27

28
29 There are four primary nitrogen configurations observed in NG: pyridinic-N, pyrrolic-N,
30
31 graphitic-N, and N-oxide (Figure 1).^{13, 20, 33, 34} Pyridinic-N and pyrrolic-N are located on
32
33 graphene edges, the pyridinic structure is sp^2 hybridized and bonded to two carbon atoms while
34
35 the pyrrolic structure is sp^3 hybridized and incorporated into five-membered ring. Graphitic
36
37 valley and center nitrogen configurations refer to the sp^3 N atoms within the six-membered
38
39 carbons. N-oxide refers to the nitrogen bonded with two carbon atoms and one oxygen atom.
40
41 These nitrogen bonding types play profoundly different roles in tuning the graphene electronic
42
43 properties, providing a *p*-type doping (electron-deficient, higher tendency to withdraw electrons)
44
45 by pyridinic- and pyrrolic-N and a *n*-type doping (electron-rich, higher tendency to donate
46
47 electrons) by graphitic-N.^{16, 22, 23} The type of nitrogen introduced into the carbon lattice of our
48
49 samples was tailored using thermal annealing at different temperatures (650, 800, 950 °C) after
50
51
52
53
54
55
56
57
58
59
60

1
2
3 the hydrothermal reaction, leveraging different thermal stabilities of the N-types: graphitic-N >
4 pyridinic-N > pyrrolic-N.^{14, 48}
5
6

7
8 **<Figure 1>**
9

10 XPS was used to quantify the amount and distribution of N-types on our different samples
11 (data compiled in Table 1). The results confirm that nitrogen was successfully doped to the
12 graphene lattice and that a systematic distribution of the four nitrogen configurations was
13 achieved. A 9.17% and 6.86% total nitrogen is introduced into the graphene sheets for NG-U and
14 NG-UA, respectively. Upon annealing, the total nitrogen content decreases to 5.70% for NG-U-
15 950 and 3.84% for NG-UA-800, suggesting the removal of thermally unstable N species at these
16 higher temperatures. The annealing treatment enables a self-arrangement and temperature-
17 favored competition among different N-types (see details below on the conversion between N-
18 types). In addition, lower percent oxygen (O%) is observed for NG-U and NG-UA than for the
19 rGO sample, suggesting that the N-doping process reduces oxygen functional groups on GO as a
20 result of competitive doping between oxygen and nitrogen precursors.³⁸
21
22
23
24
25
26
27
28
29
30
31
32
33
34

35 **<Table 1>**
36

37 To quantify the relative amount of each N-type, the N1s spectra of NG samples were
38 deconvoluted into four components (Figure S1). The binding energies for three main peaks
39 including pyridinic-N, pyrrolic-N, and graphitic-N were assigned by constraining the peak
40 positions to 398.7 eV (determined using a standard poly(3,5 pyridine)), 399.8 eV (determined
41 using a standard polypyrrole), and 401.7 eV⁴⁹ (based on a previous study on a nearly pure
42 graphitic-N doped graphene), respectively. The remaining small region centered at 404 eV was
43 assigned to N-oxide, which is in good agreement with the literature.^{15, 33, 34, 36, 50} The N-bonding
44 configurations in the NG samples fabricated by the one-step hydrothermal method with either
45
46
47
48
49
50
51
52
53
54
55
56
57
58
59
60

1
2
3 urea or uric acid (NG-U and NG-UA) are composed mainly of pyrrolic-N. The subsequent
4 thermal treatment shifts the predominant N to pyridinic-N, for all samples. A decrease in percent
5 pyrrolic-N and pyridinic-N and increase in graphitic-N is observed after a further increase in the
6 annealing temperature. These shifts occur due to different thermal stabilities of N-types, with
7 graphitic-N being the most stable.^{14, 48} This conversion from pyrrolic-N to pyridinic-N or
8 graphitic-N shifts the material propensity toward both electrochemical and biological activities.

9
10
11
12
13
14
15
16
17 *Raman spectra reveal the changes in defect density and the shift between n- and p-type doping.*

18 Raman spectroscopy is used to characterize the changes in defect density by comparing the
19 intensity ratio of the D and G peak (I_D/I_G). It can also be used to differentiate the doping types
20 (*n*- or *p*-type) based on the shift of G peak position (Figure 2).^{23, 51, 52} The broad bump-like 2D
21 region ($2400\text{-}3250\text{ cm}^{-1}$) is observed for all samples (Figure S2), which is indicative of the high
22 defect density regime.^{7, 53, 54} In this regime, an increase of I_D/I_G indicates a decrease in defect
23 density as opposed to the low defect density regime where the increase of I_D/I_G corresponds to an
24 increase in defect density.^{7, 53, 54} A higher I_D/I_G is noted for all NG samples compared to rGO,
25 suggesting that N-doping reduces the defects by removing oxygen groups restoring the
26 conjugated graphene structure. NG-U has the highest defect level (i.e., lowest I_D/I_G ratio) among
27 all doped samples. The annealing process after one-step hydrothermal process decreases the
28 defect level through the reduction of N and O functionalities. The annealing at higher
29 temperature does not significantly change the content of defects between NG-U-650 and NG-U-
30 950, while NG-UA-800 exhibits a lower defect level than NG-UA-650.

31
32
33
34
35
36
37
38
39
40
41
42
43
44
45
46
47
48
49 <Figure 2>

50 The effects of doping and the resultant compressive and tensile strain in graphene are possible
51 origins for the shift of Raman peaks.⁵² The shift of G peak position is a fingerprint of the
52
53
54
55
56
57
58
59
60

1
2
3 concentration of charge carriers and dopants.⁵² The downshift of G peak position could be
4 attributed to the incorporation of N atoms leading to *n*-type doping (graphitic-N) while an upshift
5 is observed for *p*-type doping (pyridinic-N, pyrrolic-N).^{16, 55} An upshift in the G peak at 1600
6 cm⁻¹ is observed for the rGO sample compared to the value (~1580 cm⁻¹) reported for pure
7 graphene without significant defects (i.e., no D peak is observed).⁵¹ This is due to the presence of
8 residual oxygen functional groups causing a *p*-doping effect.⁵⁰ Upon being doped with N, the
9 downshift of G peak position in NG-U and NG-UA suggests that the incorporation of N atoms
10 reduce the effects of *p*-doping. A further downshift of G peak position is noted for the annealed
11 samples, indicating an overall enhanced *n*-doping resulting from a higher content of graphitic-N,
12 which agrees with XPS results.
13
14
15
16
17
18
19
20
21
22
23
24
25

26
27 *No notable changes in graphene morphology are observed upon N-doping.* TEM images of
28 synthesized samples (Figure 3), including undoped graphene (rGO), N-doped graphene (NG-U
29 and NG-UA), and N-doped graphene with a further thermal treatment (NG-U-950 and NG-UA-
30 800), show randomly compact and wrinkled multilayer graphene nanosheets. The structure of
31 graphene morphology is well maintained after N-doping, and there is no apparent morphological
32 difference among the five samples, suggesting that N-doping with different nitrogen precursors
33 by the hydrothermal method and the subsequent thermal treatment do not influence the graphene
34 morphology. The distribution of elements in the NG samples is shown by chemical mapping
35 using STEM-EDS. A uniform distribution of N is shown in Figure 3f-i, and that of C and O in
36 Figure S3.
37
38
39
40
41
42
43
44
45
46
47
48
49

50 <Figure 3>

51
52 **Identifying oxidative stress as the dominant mechanism of biological activity**
53
54
55
56
57
58
59
60

1
2
3 The predominant mechanisms that are proposed to contribute to adverse biological impacts of
4 graphene-based nanomaterials include chemical and physical pathways. Chemical mechanisms
5 primarily refer to oxidative-stress induced by the graphene material, including direct redox
6 reaction at bio-interfaces or indirect via the production of reaction oxygen species (ROS).^{40, 56-59}
7
8 Physical mechanisms include membrane-disruption imposed by the physical interaction with the
9 graphene edges^{56, 59-61} and the wrapping or trapping of organisms given the unique thin 2D
10 structure of graphene sheets.^{40-43, 59} The relative contribution of each mechanism and the ability
11 to manipulate their magnitude of impact remains unresolved. Herein, different NG samples were
12 found to exhibit different propensities for GSH oxidation and *E. coli* K12 inactivation, with the
13 oxidative stress identified to be the dominant mechanism.
14
15
16
17
18
19
20
21
22
23
24
25

26 The oxidative potential of the NG sample set was assessed by the acellular oxidation of GSH.
27 GSH is a cellular antioxidant and plays a major role in maintenance of a healthy redox
28 balance^{58, 62} by oxidizing to its disulfide form (glutathione disulfide, GSSG)⁶² to protect against
29 exogenous oxidative agents, such as ROS.^{63, 64} The balance of GSH and GSSG serves as a
30 predictor of the ability to defend oxidative stress.⁶⁵ Due to the close relevance of GSH to
31 oxidative stress, GSH oxidation is commonly used to probe the level of oxidative stress imparted
32 by graphene-based nanomaterials.^{7, 40, 56, 58} Further, given that oxidative stress has been shown to
33 be a major mechanism for bacterial cytotoxicity of graphene-based nanomaterials,^{41, 56} the
34 depletion of GSH can be correlated with antibacterial activity wherein the effects of bacterial
35 inactivation result from the chemical pathway (i.e., by oxidative stress).
36
37
38
39
40
41
42
43
44
45
46
47
48

49 GSH was exposed to rGO and NG samples for 6 h and the measurement of non-oxidized
50 portion of GSH was conducted using Ellman's assay at 1, 2.5, 4, and 6 h. Due to the high activity
51 of NG-UA-650 and -800, additional data was collected at 0.25 and 0.5 h. The magnitude of GSH
52
53
54
55
56
57
58
59
60

1
2
3 oxidation is different for the differentially treated samples (Figure 4a), while the relative trend
4 between the samples is maintained at all measured timepoints. The kinetic rate constants (k , mL
5 $\text{mg}^{-1} \text{h}^{-1}$) determined from the slope of the linear curve fits ($\ln [\text{GSH}]$ versus time, Figure S4)
6 follow the order: NG-U-650 (2.30) < rGO (2.84) < NG-U-950 (7.33) < NG-U (7.97) < NG-UA
7 (13.14) < NG-UA-650 (94.40) < NG-UA-800 (208.27), with a strong fit to the first-order kinetic
8 model ($R^2 > 0.98$). The effect of nitrogen precursors (urea and uric acid) on the oxidative
9 capacity of samples toward GSH is significant; the samples with uric acid as the N-precursor
10 (NG-UA, NG-UA-650 and -800) oxidize GSH considerably faster than those prepared from urea
11 (NG-U, NG-U-650 and -950). Annealing temperatures are also found to influence the oxidative
12 potential of NG samples. As the annealing temperature increases from 650 °C to 800 °C (for uric
13 acid samples) and from 650 °C to 950 °C (for urea samples), GSH oxidation increases from 83%
14 to 100% at 0.5 h and from 46% to 88% at 6 h for samples synthesized from uric acid and urea,
15 respectively. Interestingly, while the annealed samples within the uric acid sample set (NG-UA-
16 650 and -800) induce a higher GSH loss than the non-annealed sample (NG-UA), this trend does
17 not hold for urea samples. NG-U causes similar GSH oxidation compared to NG-U-950, both of
18 which are significantly higher than NG-U-650. The combined GSH oxidation results
19 demonstrate that the prepared samples, with different C:N compositions and distributions of N-
20 types, have different oxidative potentials suggesting induction of differential magnitudes of
21 oxidative stress to bacterial cells.
22
23
24
25
26
27
28
29
30
31
32
33
34
35
36
37
38
39
40
41
42
43
44
45

46 <Figure 4>

47
48
49 The antibacterial activity of the NG sample set to the model bacterium *E. coli* K12 was
50 evaluated. A similar trend is observed among the samples for *E. coli* K12 inactivation (Figure 4b)
51 and GSH oxidation (Figure 4a). For example, increasing the annealing temperature leads to a
52
53
54
55
56
57
58
59
60

1
2
3 higher magnitude of cytotoxicity (NG-U-950 > NG-U-650 and NG-UA-800 > NG-UA-650) and
4
5 the two annealed uric acid samples (NG-UA-650 and -800) demonstrate the highest GSH
6
7 oxidation and high bacterial inactivation. The similar trends suggest that while physical
8
9 proximity of the graphene material to the bacteria cell is necessary to induce a response, the
10
11 dominant mechanism of cytotoxicity is chemical in nature rather than physical puncturing (see
12
13 additional explanation below). The hydrothermal and thermal annealing treatments do not
14
15 significantly affect the structure and morphology of the prepared NG samples (see Figure 3),
16
17 suggesting that the physical disruption mechanism induced by sharp edges of graphene (if it
18
19 exists) is not likely explanations for the observed differences in bacterial cytotoxicity. Rather, the
20
21 difference in the observed cytotoxic potentials among our samples (e.g., a > 90% loss of cell
22
23 viability for NG-UA-650 and -800 versus a < 5% of that for rGO, NG-U-650, and NG-UA)
24
25 indicates that cell damage is induced through oxidative stress mechanisms rather than physical
26
27 disruption.
28
29
30
31
32

33 The potential influence of a physical wrapping mechanism has been proposed and can
34
35 confound conventional culturing approaches to evaluating cytotoxicity by inhibiting bacterial
36
37 proliferation on agar plates. The effect of wrapping is typically investigated by releasing trapped
38
39 cells through a mild bath sonication prior to plating.⁴⁰⁻⁴⁴ In agreement with previous studies^{41, 42,}
40
41
42⁴⁴, cell entrapment by the NG samples is not observed as there is no statistically significant ($P >$
43
44 0.05) decrease in cell viability loss before and after sonication (Figure 4b). The combined results
45
46 from the GSH oxidation and the cell inactivation support the dominant role of oxidative stress in
47
48 the biological reactivity of our NG samples and their diverse oxidative potential.
49
50

51 **Evaluation of oxygen reduction reaction (ORR) and oxygen evolution reaction (OER)**
52
53 **validates different electron transfer properties as a function of N-type**
54
55
56
57
58
59
60

1
2
3 ORR and OER are electrochemical processes that underlie clean energy technologies,
4 including water splitting, fuel cells, and metal-air batteries.^{6, 13, 17} Graphene-based nanomaterials
5 have been pursued as metal-free catalysts to replace the noble-metal commercial catalysts (e.g.,
6 Pt, Ir, Ru) that are scarce and high-cost.^{6, 12, 13, 17} Further, nitrogen-doped graphene has been
7 extensively studied in the field of ORR and OER.^{12, 13, 35-37} As such, ORR and OER are used in
8 this work to represent the desired functional performance of NG materials. Also, given the
9 importance of oxygen and electron transfer in the mechanisms of biological activities,⁷⁻⁹ the
10 evaluation of ORR and OER activities of NG will be useful for a better understanding of the
11 underlying mechanism of interaction at the bio-interface. Herein, the evaluation of functional
12 electrochemical activities, ORR and OER, of NG samples validate different electron transfer
13 properties as a function of nitrogen type.
14
15
16
17
18
19
20
21
22
23
24
25
26
27

28 The enhanced ORR and OER activities are driven by properties of graphene-based materials,
29 including the (i) electrical conductivity for electron transport within the graphene plane,⁶⁶⁻⁶⁸ (ii)
30 defects (topological and edge defects) that offer active sites,^{69, 70} (iii) electroactive surface area
31 available for accessing active sites,⁶⁸ and (iv) presence of functionalities (e.g., pyridinic-N,
32 graphitic-N) that induce active sites for accelerating the adsorption of targets (and the
33 intermediates) and favor electron transport for the reaction.^{36, 37, 71} While the ORR reduces O₂ to
34 H₂O, OER can be considered the opposite reaction in which H₂O oxidizes to O₂. Considering
35 this inherently different mechanisms between ORR and OER, the active N moieties in NG to
36 influence each activity will depend on their ability to donate or withdraw electrons.
37
38
39
40
41
42
43
44
45
46
47
48

49 ORR and OER are commonly carried out in a hydrodynamic condition. This enhances mass
50 transfer by inducing convection so that steady-state diffusion is achieved, enabling elucidation of
51 the kinetics and the mechanism of electrode reactions with high precision measurements. RRDE
52
53
54
55
56
57
58
59
60

1
2
3 and RDE measurements were performed for ORR and OER, respectively.⁷² Both experiments
4 were conducted in alkaline media due to the advantages in terms of a decreased overpotential
5 and a less corrosive environment compared to the process in acidic media.⁷³ Enhancement in
6 ORR and OER activities is typically represented by a more positive onset potential and a higher
7 absolute value of the current density on the potential-current polarization curves.
8
9

10 Trends in ORR polarization curves for rGO and NG samples are displayed in Figure 5a with
11 the Pt/C curve shown for comparison. While rGO and NG samples demonstrate a poor ORR
12 activity compared to Pt/C (as the reference), different ORR activity is observed between
13 samples, with the trend in onset potential: NG-U-650 (-0.189 V) < rGO (-0.179 V) < NG-UA (-
14 0.169 V) ~ NG-UA-650(-0.169 V) < NG-U-950 (-0.164 V) < NG-U (-0.159 V) < NG-UA-800 (-
15 0.149 V). After the one-step hydrothermal synthesis, NG-U demonstrates a better
16 electrochemical activity than NG-UA, indicating there are different interactions between urea
17 and uric acid with GO during the hydrothermal synthesis. The subsequent annealing process
18 results in a more pronounced increase in the electrochemical reactivity of samples within the uric
19 acid precursor set than that within the urea precursor set.
20
21
22
23
24
25
26
27
28
29
30
31
32
33
34
35
36

37 <Figure 5>

38 The electron transfer number (n) and the H_2O_2 yield (H_2O_2 %) were calculated by employing
39 RRDE (Figure S5). ORR in alkaline media can occur by either a two-electron ($O_2 + H_2O + 2e^-$
40 $\rightarrow HO_2^- + OH^-$, $HO_2^- + H_2O + 2e^- \rightarrow 3OH^-$) or a four-electron ($O_2 + 2H_2O + 4e^- \rightarrow 4OH^-$)
41 pathway thus, a higher n represents a lower H_2O_2 yield. The four-electron pathway is
42 advantageous for energy applications because the H_2O_2 intermediates produced in the two-
43 electron pathway will deteriorate the catalysts and lead to a decline in the O_2 utilization rate.⁷⁴ At
44 the potential ranging from -0.4 to -1.0 V, the n calculated for all samples falls within a range of
45
46
47
48
49
50
51
52
53
54
55
56
57
58
59
60

1
2
3 3.5 (25% H₂O₂) to 3.9 (5% H₂O₂), suggesting a predominant 4-electron oxygen reduction
4 pathway. In general, NG-UA and NG-UA-650 show a lower n than rGO over this potential range
5 while other samples enhance n , which suggests that the C:N compositions and distribution of N-
6 types influences the reduction pathway.
7
8
9

10
11
12 The capacity of graphene materials to catalyze ORR depends on the defect density because
13 defect sites can enhance the O₂ adsorption.⁵⁸ The higher defect density in NG-U explains the
14 favorable reactivity toward ORR. While annealing decreases the defect density and subsequently
15 suppresses the ORR activity, we observe an increasing ORR trend between NG-U-650 and NG-
16 U-950 (having similar defect density), and between NG-UA-650 and NG-UA-800 (the latter
17 having a lower defect density). This indicates that another property of these materials is involved
18 in the observed difference in ORR activity. The proportion of different N-types, rather than the
19 nitrogen content on the graphene, has been proposed to play an important role in the facilitation
20 of electrocatalytic activity.^{37, 71, 75, 76} Graphitic-N possesses the electron-donating characteristic^{16,}
21 ^{22, 23} and greater charge carrier transport over other N-types.^{21, 22} Graphitic-N atoms can lower the
22 O₂ adsorption barrier by decreasing the repulsive interaction between graphene π electrons and
23 lone pair electrons of O₂,^{71, 76} and can facilitate the donation of electrons to the adsorbed O₂ to
24 form OOH species,^{37, 77} both of which are key steps to enhance the reduction of O₂ in alkaline
25 solution. As a result, the samples annealed at higher temperatures demonstrate enhanced
26 reactivity toward ORR due to the increase in the content of graphitic-N (Figure 5b).
27
28
29
30
31
32
33
34
35
36
37
38
39
40
41
42
43
44
45
46

47 The electrocatalytic activity of the annealed samples within urea and uric acid precursor sets
48 was investigated toward OER to determine whether the predicted opposing trend is observed as
49 predicted; samples with more pyridinic-N would have a greater propensity towards OER. Indeed,
50 the opposite trend (Figure 5c and 5d) is observed for OER compared to that for ORR. The
51
52
53
54
55
56
57
58
59
60

1
2
3 samples annealed at higher temperatures (having 2.69% and 1.96 % pyridinic-N for NG-U-950
4 and NG-UA-800, respectively) demonstrate lower OER activity in terms of the current density
5 than that at lower temperatures (having 3.33% and 2.18% pyridinic-N for NG-U-650 and NG-
6 UA-650). The carbon adjacent to electron-donating graphitic-N atoms possess a partial negative
7 charge (δ^-) and therefore can serve as nucleophiles. This behavior is unfavorable for the
8 adsorption of intermediates necessary for water oxidation in the alkaline media (e.g., OH^- , OOH^-
9).^{37, 75} Carbon atoms adjacent to electron-withdrawing pyridinic-N atoms carry a partial positive
10 charge (δ^+), thus serving as electrophiles facilitating the adsorption of intermediates necessary
11 for water oxidation (e.g., OH^- , OOH^-).^{37, 78} In addition, the polarized pyridinic-N (δ^-) is not
12 favorable for the reduction of O_2 due to its high density of N lone pair electrons that cause strong
13 repulsive interaction with the O_2 approaching its adjacent carbon atoms.⁷¹ Consequently, the
14 samples annealed at higher temperatures demonstrate lower reactivity toward OER owing to the
15 decrease in the pyridinic-N content.

16
17
18
19
20
21
22
23
24
25
26
27
28
29
30
31
32
33 While samples annealed with uric acid (NG-UA-650 and -800) contain lower percentage of
34 graphitic-N and pyridinic-N than those within urea sample set (NG-U-650 and -950), the uric
35 acid sample set presents an overall higher ORR and OER (Figure 5b and 5d). This observation
36 suggests another property in contributing to the sample activity and is attributed to the higher
37 surface area of the uric acid materials (Figure S6). The Brunauer-Emmett-Teller (BET) surface
38 area for NG-UA-800 is $549.3 \text{ m}^2 \text{ g}^{-1}$ and $428.2 \text{ m}^2 \text{ g}^{-1}$ for NG-U-950, enhancing access to the
39 active sites that facilitate the electrocatalytic activities. The observed differences in BET surface
40 area is maintained when the respective materials are dispersed (see additional details below).

41
42
43
44
45
46
47
48
49
50
51 Taken together, the characterization data indicate that multiple physicochemical properties of
52 NG influence the electrochemical performance (here, ORR and OER activities). While the
53
54
55
56
57
58
59
60

1
2
3 consequential material properties that result from N-doping (e.g., defect density, surface area)
4 influence ORR and OER synchronously, opposite trends observed for ORR and OER highlight
5 the significant role of N-types in mediating these two electrochemical activities. While electron-
6 donating graphitic-N and electron-withdrawing pyridinic-N are effective promoters for ORR and
7 OER, respectively, the defect density and surface area that result from different preparation
8 methods (precursors and annealing temperatures) further contribute to the material activity.
9

10
11
12
13
14
15
16
17 **The similarity between glutathione (GSH) oxidation and oxygen reduction reaction (ORR)**
18 **reveals the role of graphitic-N as the active site in oxidative stress related bioactivity**
19

20
21
22 The evaluation of biological activity of our NG sample set highlights the essential role of
23 oxidative stress at bio-interfaces and affirms that the oxidation of GSH is a good predictor of
24 oxidative stress delivered by our NG samples. Previous studies propose that graphene family
25 nanomaterials catalyze GSH oxidation through electron transfer with dissolved oxygen at the
26 defect sites.^{42, 58} The dissolved oxygen (O_2) reacts with active defect sites on graphene forming
27 surface-bound oxygen intermediates (e.g., superoxide anion O_2^- , hydroperoxide OOH) that can
28 oxidize GSH or be released to the bulk solution to form reactive oxygen species (ROS) that react
29 with GSH.⁵⁸ The rate-limiting step for the oxidation of GSH is the formation of the surface oxide
30 intermediates (O_2^- , OOH), similar to mechanism for ORR on the electrode surface in alkaline
31 solution. Since O_2 has a high bond dissociation energy, it is not uniformly favorable and requires
32 the formation of intermediates (O_2^- , OOH) that have lower bond dissociation energy.^{73, 75} As
33 such, the oxidation of GSH and ORR share a similar mechanism, both of which are dominated
34 by O_2 -mediated catalytic process to reduce O_2 that starts with O_2 adsorption on the active sites of
35 graphene materials.^{58, 73} It is thus expected that graphitic-N can influence the capacity of NG to
36 oxidize GSH, as it does for ORR.
37
38
39
40
41
42
43
44
45
46
47
48
49
50
51
52
53
54
55
56
57
58
59
60

1
2
3 Similar trends are observed for the oxidation of GSH and the ORR activity within each N-
4 precursor set (urea versus uric acid in Figure 6a). As with the ORR trends described above, the
5 important contribution of defects to the oxidization of GSH is underlined by the higher defect
6 density in NG-U than the two annealed samples (NG-U-650 and -950, see Figure 2). The
7 samples annealed at higher temperatures within each N-precursor show an increased oxidative
8 potential toward GSH, which is attributed to the increase in the percent of graphitic-N. Yet
9 similar to the ORR trend described above, the samples prepared with the uric acid precursor have
10 lower amounts of graphitic-N than those prepared with urea while exhibiting higher oxidative
11 potential, which is believed to result from the increase in available surface area. Since the GSH
12 assay is performed in the aqueous media, the dispersed surface area of the samples was evaluated
13 by the adsorption of methylene blue (Figure 6b). This approach is regarded as a standard method
14 for measuring the surface area of graphitic materials in the aqueous phase.^{45, 79} Overall, a higher
15 surface area corresponds with a better dispersion, which is observed for the uric acid samples. A
16 visual comparison of their dispersion in water is shown in Figure S7. The increase in the thermal
17 annealing temperatures induces a reduction in the dispersed surface area in both sample sets.
18 This is caused by the removal of surface functionalities, which promotes aggregation of the
19 samples in suspension, thus decreasing the available dispersed surface area.
20
21
22
23
24
25
26
27
28
29
30
31
32
33
34
35
36
37
38
39
40
41

42 <Figure 6>

43
44 Collectively, the data supports multiple factors synergistically influencing the NG-mediated
45 oxidation of GSH. In addition to the defect density and dispersed surface area, uncovering the
46 role of graphitic-N in both ORR and GSH oxidation elucidates the underlying mechanisms of
47 oxidative-stress induced biological activity. The similarities in ORR and GSH trends suggests
48
49
50
51
52
53
54
55
56
57
58
59
60

1
2
3 the potential to employ electrochemical tools to evaluate the relative bioactivity of graphene
4 materials via chemical pathways.
5
6

7 **The opportunity to tailor functional performance and inherent hazard outcomes**

8
9
10 Sustainable design of nanomaterials defines a proactive approach to advance new applications
11 while reducing the potential to introduce hazards to human health and the environment.^{11, 80}
12
13 Results from this study demonstrate that governing N-types are distinct for electrochemical
14 applications given their unique electronic properties. Specifically, graphitic-N is responsible for
15 the reduction of oxygen (ORR) while pyridinic-N is responsible for water oxidation (OER). This
16 suggests the ability to tune performance based on chemical composition, which we demonstrate
17 is possible using different N-precursors and annealing temperatures. While the goal of a
18 sustainable design approach is to enhance functional performance while reducing inherent
19 bioactivity (GSH oxidation, cytotoxicity), a possible outcome is that the same material property
20 modulates both outcomes. This was the result in our previous research on GO/rGO^{7,8,9} as well as
21 in this study for NG and ORR performance. Yet, in studying N-doped graphene herein, we
22 discovered that the ability to decouple functional performance and bioactivity will depend on the
23 desired performance outcome (i.e., ORR versus OER). For example, the functional performance
24 of OER is facilitated by pyridinic-N and the samples with high pyridinic-N have lower oxidative
25 potential, thus suggesting a path towards enhanced performance without high bioactivity. While
26 we used two approaches to modulating N-types of NG, there are many more options that enable
27 further control of N doping to obtain closer to pure graphitic or pyridinic C-N bonding
28 configuration^{49, 71} and advance the intended rational sustainable design for their applications.
29
30
31
32
33
34
35
36
37
38
39
40
41
42
43
44
45
46
47
48
49
50

51 **CONCLUSIONS**

52
53
54
55
56
57
58
59
60

1
2
3 The type of N that is incorporated in the graphene structure depends on how the sample is
4 prepared, including the nature of N precursors and annealing temperatures. The different amount
5 of doped N and the relative abundance of N-types differentially influence biological and
6 electrochemical activities. Defect density and surface area are consequential properties that result
7 from changes in N-content and work in concert with chemical composition to modulate both
8 activities. While this work identifies these three properties to govern the measured outcomes
9 (i.e., GSH oxidation, bacterial inactivation, ORR, and OER), the contribution of each property to
10 each outcome differs. For example, the trends in GSH oxidation and bacteria inactivation for the
11 uric acid and urea sample sets are similar, yet the magnitude of the difference between individual
12 samples differs for these two measured biological activities (Figure 4a versus 4b). These findings
13 elucidate the opportunity to tune (un)desired properties and material activities by modifying
14 graphene chemistry.
15
16
17
18
19
20
21
22
23
24
25
26
27
28
29

30 While both electrochemical and biological activities are controlled by a balance between
31 multiple properties, the type of N has an overarching effect. Electron-donating graphitic-N is
32 responsible for ORR and O₂-mediated oxidative stress in bioactivity while electron-withdrawing
33 pyridinic-N is responsible enhancement in OER. Identification of N active sites for biological
34 activities is useful to guide the development of N-doped graphene materials for their biomedical
35 and bioanalytical applications. From the perspective of rational design, N-types can be leveraged
36 as a design handle to tailor properties of graphene for specific applications while reducing or
37 maintaining minimal adverse biological effects.
38
39
40
41
42
43
44
45
46
47
48

49 Finally, there is growing evidence of the correlation between electrochemical activity and
50 biological reactivity of carbon nanomaterials including multi-walled carbon nanotubes,^{8, 9}
51 graphene oxide,⁷ and N-doped graphene (in the present work). Uncovering the underlying
52
53
54
55
56
57
58
59
60

1
2
3 electronic nature of graphene, including the ability to engage in electron exchange and transport,
4
5 is critical to informing the ability to rationally design graphene materials for electrochemical
6
7 applications while also advancing predictive toxicity capabilities.
8
9

10 **SUPPORTING INFORMATION**

11
12
13 The Supporting Information is available free of charge on the RSC publications website,
14
15 including the methodological details of material characterization techniques; the deconvoluted
16
17 XPS N1s spectra to determine the distribution of N-types (Figure S1); the Raman spectra
18
19 including D, G peaks and 2D region (Figure S2); the STEM-EDS elemental maps showing the
20
21 distribution of C and O on the graphene (Figure S3); the plots of $\ln [\text{GSH}]$ versus time to
22
23 calculate the kinetic rates of GSH oxidation (Figure S4); the electron transfer number n and the
24
25 yield of H_2O_2 determined by RRDE (Figure S5); the nitrogen adsorption-desorption isotherms to
26
27 investigate the BET surface area (Figure S6); and the photographs comparing the dispersion
28
29 behavior of urea and uric acid samples (Figure S7).
30
31
32
33

34 **CONFLICTS OF INTEREST**

35
36
37 There are no conflicts to declare.
38
39

40 **ACKNOWLEDGEMENTS**

41
42 The authors acknowledge generous financial support provided by the National Science
43
44 Foundation CBET Award No. 1709031 and the University of Pittsburgh Central Research
45
46 Development Fund. The authors thank Dr. Howard Fairbrother for his time, insight, and
47
48 guidance provided for robust XPS deconvolution quantifying different N-types, and Dr. Yahui
49
50 Yang for assistance with the BET surface area measurement.
51
52
53
54
55
56
57
58
59
60

REFERENCES

1. McWilliams, A., The Maturing Nanotechnology Market: Products and Applications. *BCC Research, NAN031G* 2016.
2. Jariwala, D.; Sangwan, V. K.; Lauhon, L. J.; Marks, T. J.; Hersam, M. C., Carbon Nanomaterials for Electronics, Optoelectronics, Photovoltaics, and Sensing. *Chem. Soc. Rev.* 2013, **42** (7), 2824-2860.
3. Hou, J.; Shao, Y.; Ellis, M. W.; Moore, R. B.; Yi, B., Graphene-Based Electrochemical Energy Conversion and Storage: Fuel Cells, Supercapacitors and Lithium Ion Batteries. *Phys. Chem. Chem. Phys.* 2011, **13** (34), 15384-402.
4. Zheng, H.; Ma, R.; Gao, M.; Tian, X.; Li, Y.-Q.; Zeng, L.; Li, R., Antibacterial Applications of Graphene Oxides: Structure-Activity Relationships, Molecular Initiating Events and Biosafety. *Sci. Bull.* 2017, **63** (2), 133-142.
5. Reina, G.; González-Domínguez, J. M.; Criado, A.; Vázquez, E.; Bianco, A.; Prato, M., Promises, Facts and Challenges for Graphene in Biomedical Applications. *Chem. Soc. Rev.* 2017, **46** (15), 4400-4416.
6. Hu, C.; Dai, L., Carbon - Based Metal - Free Catalysts for Electrocatalysis beyond the ORR. *Angew. Chem. Int. Ed.* 2016, **55** (39), 11736-11758.
7. Wang, Y.; Gilbertson, L. M., Informing Rational Design of Graphene Oxide through Surface Chemistry Manipulations: Properties Governing Electrochemical and Biological Activities. *Green Chem.* 2017, **19** (12), 2826-2838.
8. Pasquini, L. M.; Sekol, R. C.; Taylor, A. D.; Pfefferle, L. D.; Zimmerman, J. B., Realizing Comparable Oxidative and Cytotoxic Potential of Single- and Multiwalled Carbon Nanotubes through Annealing. *Environ. Sci. Technol.* 2013, **47** (15), 8775-8783.
9. Gilbertson, L. M.; Goodwin Jr, D. G.; Taylor, A. D.; Pfefferle, L.; Zimmerman, J. B., Toward Tailored Functional Design of Multi-Walled Carbon Nanotubes (MWNTs): Electrochemical and Antimicrobial Activity Enhancement via Oxidation and Selective reduction. *Environ. Sci. Technol.* 2014, **48** (10), 5938-5945.
10. Wang, Z.; Zhu, W.; Qiu, Y.; Yi, X.; von dem Bussche, A.; Kane, A.; Gao, H.; Koski, K.; Hurt, R., Biological and Environmental Interactions of Emerging Two-Dimensional Nanomaterials. *Chem. Soc. Rev.* 2016, **45** (6), 1750-1780.
11. Gilbertson, L. M.; Zimmerman, J. B.; Plata, D. L.; Hutchison, J. E.; Anastas, P. T., Designing Nanomaterials to Maximize Performance and Minimize Undesirable Implications Guided by the Principles of Green Chemistry. *Chem. Soc. Rev.* 2015, **44** (16), 5758-5777.
12. Zhang, J.; Dai, L., Heteroatom-Doped Graphitic Carbon Catalysts for Efficient Electrocatalysis of Oxygen Reduction Reaction. *ACS Catal.* 2015, **5** (12), 7244-7253.
13. Duan, J.; Chen, S.; Jaroniec, M.; Qiao, S. Z., Heteroatom-Doped Graphene-Based Materials for Energy-Relevant Electrocatalytic Processes. *ACS Catal.* 2015, **5** (9), 5207-5234.
14. Wang, X.; Sun, G.; Routh, P.; Kim, D.-H.; Huang, W.; Chen, P., Heteroatom-Doped Graphene Materials: Syntheses, Properties and Applications. *Chem. Soc. Rev.* 2014, **43** (20), 7067-7098.
15. Wang, H.; Maiyalagan, T.; Wang, X., Review on Recent Progress in Nitrogen-doped Graphene: Synthesis, Characterization, and Its Potential Applications. *ACS Catal.* 2012, **2** (5), 781-794.
16. Liu, H.; Liu, Y.; Zhu, D., Chemical Doping of Graphene. *J. Mater. Chem.* 2011, **21** (10), 3335-3345.
17. Liu, X.; Dai, L., Carbon-Based Metal-Free Catalysts. *Nat. Rev. Mater.* 2016, **1** (11), 16064.
18. Zhang, L.; Xia, Z., Mechanisms of Oxygen Reduction Reaction on Nitrogen-Doped Graphene for Fuel Cells. *J. Phys. Chem. C* 2011, **115** (22), 11170-11176.
19. Gong, K.; Du, F.; Xia, Z.; Durstock, M.; Dai, L., Nitrogen-Doped Carbon Nanotube Arrays with High Electrocatalytic Activity for Oxygen Reduction. *Science* 2009, **323** (5915), 760-764.

- 1
2
3 20. Lai, L.; Potts, J. R.; Zhan, D.; Wang, L.; Poh, C. K.; Tang, C.; Gong, H.; Shen, Z.; Lin, J.; Ruoff, R. S.,
4 Exploration of the Active Center Structure of Nitrogen-Doped Graphene-Based Catalysts for Oxygen
5 Reduction Reaction. *Energy Environ. Sci.* 2012, **5** (7), 7936-7942.
- 6 21. Kim, H. S.; Kim, H. S.; Kim, S. S.; Kim, Y.-H., Atomistic Mechanisms of Codoping-Induced p-to
7 n-Type Conversion in Nitrogen-Doped Graphene. *Nanoscale* 2014, **6** (24), 14911-14918.
- 8 22. Usachov, D.; Vilkov, O.; Gruneis, A.; Haberer, D.; Fedorov, A.; Adamchuk, V.; Preobrajenski,
9 A.; Dudin, P.; Barinov, A.; Oehzelt, M., Nitrogen-Doped Graphene: Efficient Growth, Structure, and
10 Electronic Properties. *Nano Lett.* 2011, **11** (12), 5401-5407.
- 11 23. Schiros, T.; Nordlund, D.; Pálová, L.; Prezzi, D.; Zhao, L.; Kim, K. S.; Wurstbauer, U.; Gutiérrez,
12 C.; Delongchamp, D.; Jaye, C., Connecting Dopant Bond Type with Electronic Structure in N-Doped
13 Graphene. *Nano Lett.* 2012, **12** (8), 4025-4031.
- 14 24. Lee, W. J.; Maiti, U. N.; Lee, J. M.; Lim, J.; Han, T. H.; Kim, S. O., Nitrogen-Doped Carbon
15 Nanotubes and Graphene Composite Structures for Energy and Catalytic Applications. *Chem.*
16 *Commun.* 2014, **50** (52), 6818-6830.
- 17 25. Fan, M.; Zhu, C.; Liu, L.; Wu, Q.; Hao, Q.; Yang, J.; Sun, D., Modified PEDOT by Benign
18 Preparing N-Doped Reduced Graphene Oxide as Potential Bio-Electrode Coating Material. *Green*
19 *Chem.* 2016, **18** (6), 1731-1737.
- 20 26. Guo, M.; Li, D.; Zhao, M.; Zhang, Y.; Geng, D.; Lushington, A.; Sun, X., Nitrogen Ion Implanted
21 Graphene as Thrombo-Protective Safer and Cytoprotective Alternative for Biomedical Applications.
22 *Carbon* 2013, **61**, 321-328.
- 23 27. Boncel, S.; Müller, K. H.; Skepper, J. N.; Walczak, K. Z.; Koziol, K. K., Tunable Chemistry and
24 Morphology of Multi-Wall Carbon Nanotubes as a Route to Non-Toxic, Theranostic Systems.
25 *Biomaterials* 2011, **32** (30), 7677-7686.
- 26 28. Yang, Y.; Zhang, J.; Zhuang, J.; Wang, X., Synthesis of Nitrogen-Doped Carbon Nanostructures
27 from Polyurethane Sponge for Bioimaging and Catalysis. *Nanoscale* 2015, **7** (29), 12284-12290.
- 28 29. Zhao, M.; Cao, Y.; Liu, X.; Deng, J.; Li, D.; Gu, H., Effect of Nitrogen Atomic Percentage on N+-
29 Bombarded MWCNTs in Cytocompatibility and Hemocompatibility. *Nanoscale Res. Lett.* 2014, **9** (1),
30 142.
- 31 30. Carrero-Sanchez, J.; Elias, A.; Mancilla, R.; Arrellin, G.; Terrones, H.; Laclette, J.; Terrones, M.,
32 Biocompatibility and Toxicological Studies of Carbon Nanotubes Doped with Nitrogen. *Nano Lett.*
33 2006, **6** (8), 1609-1616.
- 34 31. Zhao, M.; Li, D.; Yuan, L.; Yue, Y.; Liu, H.; Sun, X., Differences in Cytocompatibility and
35 Hemocompatibility between Carbon Nanotubes and Nitrogen-Doped Carbon Nanotubes. *Carbon*
36 2011, **49** (9), 3125-3133.
- 37 32. Elías, A. L.; Carrero - Sánchez, J. C.; Terrones, H.; Endo, M.; Laclette, J. P.; Terrones, M.,
38 Viability Studies of Pure Carbon - and Nitrogen - Doped Nanotubes with *Entamoeba Histolytica*:
39 From Amoebicidal to Biocompatible Structures. *Small* 2007, **3** (10), 1723-1729.
- 40 33. Okada, T.; Inoue, K. Y.; Kalita, G.; Tanemura, M.; Matsue, T.; Meyyappan, M.; Samukawa, S.,
41 Bonding State and Defects of Nitrogen-Doped Graphene in Oxygen Reduction Reaction. *Chem. Phys.*
42 *Lett.* 2016, **665**, 117-120.
- 43 34. Liu, Y.; Li, J.; Li, W.; Li, Y.; Zhan, F.; Tang, H.; Chen, Q., Exploring the Nitrogen Species of
44 Nitrogen Doped Graphene as Electrocatalysts for Oxygen Reduction Reaction in Al-Air Batteries.
45 *Int. J. Hydrogen Energy* 2016, **41** (24), 10354-10365.
- 46 35. Miao, H.; Li, S.; Wang, Z.; Sun, S.; Kuang, M.; Liu, Z.; Yuan, J., Enhancing the Pyridinic N
47 Content of Nitrogen-Doped Graphene and Improving Its Catalytic Activity for Oxygen Reduction
48 Reaction. *Int. J. Hydrogen Energy* 2017, **42** (47), 28298-28308.
- 49 36. Xing, T.; Zheng, Y.; Li, L. H.; Cowie, B. C.; Gunzelmann, D.; Qiao, S. Z.; Huang, S.; Chen, Y.,
50 Observation of Active Sites for Oxygen Reduction Reaction on Nitrogen-Doped Multilayer Graphene.
51 *ACS Nano* 2014, **8** (7), 6856-6862.
- 52
53
54
55
56
57
58
59
60

37. Yang, H. B.; Miao, J.; Hung, S.-F.; Chen, J.; Tao, H. B.; Wang, X.; Zhang, L.; Chen, R.; Gao, J.; Chen, H. M., Identification of Catalytic Sites for Oxygen Reduction and Oxygen Evolution in N-Doped Graphene Materials: Development of Highly Efficient Metal-Free Bifunctional Electrocatalyst. *Sci. Adv.* 2016, **2** (4), e1501122.
38. Sheng, Z.-H.; Shao, L.; Chen, J.-J.; Bao, W.-J.; Wang, F.-B.; Xia, X.-H., Catalyst-free Synthesis of Nitrogen-Doped Graphene via Thermal Annealing Graphite Oxide with Melamine and Its Excellent Electrocatalysis. *ACS nano* 2011, **5** (6), 4350-4358.
39. Gilbertson, L. M.; Albalghiti, E. M.; Fishman, Z. S.; Perreault, F.; Corredor, C.; Posner, J. D.; Elimelech, M.; Pfefferle, L. D.; Zimmerman, J. B., Shape-Dependent Surface Reactivity and Antimicrobial Activity of Nano-Cupric Oxide. *Environ. Sci. Technol.* 2016, **50** (7), 3975-3984.
40. Perreault, F.; de Faria, A. F.; Nejati, S.; Elimelech, M., Antimicrobial Properties of Graphene Oxide Nanosheets: Why Size Matters. *ACS nano* 2015, **9** (7), 7226-7236.
41. Faria, A. F.; Perreault, F.; Elimelech, M., Elucidating the Role of Oxidative Debris in the Antimicrobial Properties of Graphene Oxide. *ACS Appl. Nano Mater.* 2018, **1** (3), 1164-1174.
42. Lu, X.; Feng, X.; Werber, J. R.; Chu, C.; Zucker, I.; Kim, J.-H.; Osuji, C. O.; Elimelech, M., Enhanced Antibacterial Activity through the Controlled Alignment of Graphene Oxide Nanosheets. *Proc. Natl. Acad. Sci.* 2017, **114** (46), E9793-E9801.
43. Akhavan, O.; Ghaderi, E.; Esfandiari, A., Wrapping Bacteria by Graphene Nanosheets for Isolation from Environment, Reactivation by Sonication, and Inactivation by Near-Infrared Irradiation. *J. Phys. Chem. B* 2011, **115** (19), 6279-6288.
44. Liu, S.; Hu, M.; Zeng, T. H.; Wu, R.; Jiang, R.; Wei, J.; Wang, L.; Kong, J.; Chen, Y., Lateral Dimension-Dependent Antibacterial Activity of Graphene Oxide Sheets. *Langmuir* 2012, **28** (33), 12364-12372.
45. Guo, H.-L.; Su, P.; Kang, X.; Ning, S.-K., Synthesis and Characterization of Nitrogen-Doped Graphene Hydrogels by Hydrothermal Route with Urea as Reducing-Doping Agents. *J. Mater. Chem. A* 2013, **1** (6), 2248-2255.
46. Sun, L.; Wang, L.; Tian, C.; Tan, T.; Xie, Y.; Shi, K.; Li, M.; Fu, H., Nitrogen-Doped Graphene with High Nitrogen Level via a One-Step Hydrothermal Reaction of Graphene Oxide with Urea for Superior Capacitive Energy Storage. *RSC Adv.* 2012, **2** (10), 4498-4506.
47. Soo, L. T.; Loh, K. S.; Mohamad, A. B.; Daud, W. R. W.; Wong, W. Y., Effect of Nitrogen Precursors on the Electrochemical Performance of Nitrogen-Doped Reduced Graphene Oxide towards Oxygen Reduction Reaction. *J. Alloys Compd.* 2016, **677**, 112-120.
48. Kundu, S.; Nagaiah, T. C.; Xia, W.; Wang, Y.; Dommele, S. V.; Bitter, J. H.; Santa, M.; Grundmeier, G.; Bron, M.; Schuhmann, W.; Muhler, M., Electrocatalytic Activity and Stability of Nitrogen-Containing Carbon Nanotubes in the Oxygen Reduction Reaction. *J. Phys. Chem. C* 2009, **113** (32), 14302-14310.
49. Wei, D.; Liu, Y.; Wang, Y.; Zhang, H.; Huang, L.; Yu, G., Synthesis of N-Doped Graphene by Chemical Vapor Deposition and Its Electrical Properties. *Nano Lett.* 2009, **9** (5), 1752-1758.
50. Lin, Z.; Waller, G.; Liu, Y.; Liu, M.; Wong, C. P., Facile Synthesis of Nitrogen - Doped Graphene via Pyrolysis of Graphene Oxide and Urea, and Its Electrocatalytic Activity toward the Oxygen - Reduction Reaction. *Adv. Energy Mater.* 2012, **2** (7), 884-888.
51. Ferrari, A. C.; Meyer, J. C.; Scardaci, V.; Casiraghi, C.; Lazzeri, M.; Mauri, F.; Piscanec, S.; Jiang, D.; Novoselov, K. S.; Roth, S.; Geim, A. K., Raman Spectrum of Graphene and Graphene Layers. *Phys. Rev. Lett.* 2006, **97** (18), 187401.
52. Zafar, Z.; Ni, Z. H.; Wu, X.; Shi, Z. X.; Nan, H. Y.; Bai, J.; Sun, L. T., Evolution of Raman Spectra in Nitrogen Doped Graphene. *Carbon* 2013, **61**, 57-62.
53. Ferrari, A. C.; Robertson, J., Interpretation of Raman Spectra of Disordered and Amorphous Carbon. *Phys. Rev. B* 2000, **61** (20), 14095.

- 1
2
3 54. Cançado, L. G.; Jorio, A.; Ferreira, E. M.; Stavale, F.; Achete, C.; Capaz, R.; Moutinho, M.;
4 Lombardo, A.; Kulmala, T.; Ferrari, A., Quantifying Defects in Graphene via Raman Spectroscopy at
5 Different Excitation Energies. *Nano Lett.* 2011, **11** (8), 3190-3196.
- 6 55. Panchakarla, L.; Subrahmanyam, K.; Saha, S.; Govindaraj, A.; Krishnamurthy, H.; Waghmare,
7 U.; Rao, C., Synthesis, Structure, and Properties of Boron - and Nitrogen - Doped Graphene. *Adv.*
8 *Mater.* 2009, **21** (46), 4726-4730.
- 9 56. Liu, S.; Zeng, T. H.; Hofmann, M.; Burcombe, E.; Wei, J.; Jiang, R.; Kong, J.; Chen, Y.,
10 Antibacterial Activity of Graphite, Graphite Oxide, Graphene Oxide, and Reduced Graphene Oxide:
11 Membrane and Oxidative Stress. *ACS Nano* 2011, **5** (9), 6971-6980.
- 12 57. Perreault, F.; Fonseca de Faria, A.; Elimelech, M., Environmental Applications of Graphene-
13 Based Nanomaterials. *Chem. Soc. Rev.* 2015, **44** (16), 5861-5896.
- 14 58. Liu, X.; Sen, S.; Liu, J.; Kulaots, I.; Geohegan, D.; Kane, A.; Poretzky, A. A.; Rouleau, C. M.; More,
15 K. L.; Palmore, G. T. R., Antioxidant Deactivation on Graphenic Nanocarbon Surfaces. *Small* 2011, **7**
16 (19), 2775-2785.
- 17 59. Zou, X.; Zhang, L.; Wang, Z.; Luo, Y., Mechanisms of the Antimicrobial Activities of Graphene
18 Materials. *J. Am. Chem. Soc.* 2016, **138** (7), 2064-2077.
- 19 60. Wu, C.; Wang, C.; Zheng, J.; Luo, C.; Li, Y.; Guo, S.; Zhang, J., Vacuolization in Cytoplasm and
20 Cell Membrane Permeability Enhancement Triggered by Micrometer-Sized Graphene Oxide. *ACS*
21 *nano* 2015, **9** (8), 7913-7924.
- 22 61. Tu, Y.; Lv, M.; Xiu, P.; Huynh, T.; Zhang, M.; Castelli, M.; Liu, Z.; Huang, Q.; Fan, C.; Fang, H.,
23 Destructive Extraction of Phospholipids from Escherichia Coli Membranes by Graphene
24 Nanosheets. *Nat. Nanotechnol.* 2013, **8** (8), 594.
- 25 62. Jones, D. P., Redox Potential of GSH/GSSG Couple: Assay and Biological Significance. In
26 *Methods Enzymol.*, Elsevier: 2002; Vol. 348, pp 93-112.
- 27 63. Smirnova, G.; Muzyka, N.; Oktyabrsky, O., Transmembrane Glutathione Cycling in Growing
28 Escherichia Coli Cells. *Microbiol. Res.* 2012, **167** (3), 166-172.
- 29 64. Owensm, R. A.; Hartman, P. E., Glutathione: a Protective Agent in Salmonella Typhimurium
30 and Escherichia Coli as Measured by Mutagenicity and by Growth Delay Assays. *Environ. Mutagen.*
31 1986, **8** (5), 659-673.
- 32 65. Schafer, F. Q.; Buettner, G. R., Redox Environment of the Cell as Viewed through the Redox
33 State of the Glutathione Disulfide/Glutathione Couple. *Free Radical Bio. Med.* 2001, **30** (11), 1191-
34 1212.
- 35 66. Zhou, R.; Zheng, Y.; Hulicova-Jurcakova, D.; Qiao, S. Z., Enhanced Electrochemical Catalytic
36 Activity by Copper Oxide Grown on Nitrogen-Doped Reduced Graphene Oxide. *J. Mater. Chem. A*
37 2013, **1** (42), 13179-13185.
- 38 67. Liang, Y.; Li, Y.; Wang, H.; Zhou, J.; Wang, J.; Regier, T.; Dai, H., Co₃O₄ Nanocrystals on
39 Graphene as a Synergistic Catalyst for Oxygen Reduction Reaction. *Nat. Mater.* 2011, **10** (10), 780-
40 786.
- 41 68. Jiang, Z.-J.; Jiang, Z., Interaction Induced High Catalytic Activities of CoO Nanoparticles
42 Grown on Nitrogen-Doped Hollow Graphene Microspheres for Oxygen Reduction and Evolution
43 Reactions. *Sci. Rep.* 2016, **6**, 27081.
- 44 69. Bagri, A.; Mattevi, C.; Acik, M.; Chabal, Y. J.; Chhowalla, M.; Shenoy, V. B., Structural Evolution
45 during the Reduction of Chemically Derived Graphene Oxide. *Nat. Chem.* 2010, **2** (7), 581-587.
- 46 70. Gómez-Navarro, C.; Meyer, J. C.; Sundaram, R. S.; Chuvilin, A.; Kurasch, S.; Burghard, M.;
47 Kern, K.; Kaiser, U., Atomic Structure of Reduced Graphene Oxide. *Nano Lett.* 2010, **10** (4), 1144-
48 1148.
- 49 71. Luo, Z.; Lim, S.; Tian, Z.; Shang, J.; Lai, L.; MacDonald, B.; Fu, C.; Shen, Z.; Yu, T.; Lin, J.,
50 Pyridinic N Doped Graphene: Synthesis, Electronic Structure, and Electrocatalytic Property. *J.*
51 *Mater. Chem.* 2011, **21** (22), 8038-8044.
- 52
53
54
55
56
57
58
59
60

- 1
2
3 72. Bard, A. J.; Faulkner, L. R., Methods Involving Forced Convection-Hydrodynamic Methods. In
4 *Electrochemical Methods: Fundamentals and Applications*, 2nd ed.; Wiley: New York, 2001; pp 331-
5 364.
- 6 73. Ge, X.; Sumboja, A.; Wu, D.; An, T.; Li, B.; Goh, F. W. T.; Hor, T. S. A.; Zong, Y.; Liu, Z., Oxygen
7 Reduction in Alkaline Media: From Mechanisms to Recent Advances of Catalysts. *ACS Catal.* 2015, **5**
8 (8), 4643-4667.
- 9 74. Ferrero, G. A.; Preuss, K.; Marinovic, A.; Jorge, A. B.; Mansor, N.; Brett, D. J. L.; Fuertes, A. B.;
10 Sevilla, M.; Titirici, M.-M., Fe-N-Doped Carbon Capsules with Outstanding Electrochemical
11 Performance and Stability for the Oxygen Reduction Reaction in Both Acid and Alkaline Conditions.
12 *ACS Nano* 2016, **10** (6), 5922-5932.
- 13 75. Okamoto, Y., First-Principles Molecular Dynamics Simulation of O₂ Reduction on Nitrogen-
14 Doped Carbon. *Appl. Surf. Sci.* 2009, **256** (1), 335-341.
- 15 76. Niwa, H.; Horiba, K.; Harada, Y.; Oshima, M.; Ikeda, T.; Terakura, K.; Ozaki, J.-i.; Miyata, S., X-
16 Ray Absorption Analysis of Nitrogen Contribution to Oxygen Reduction Reaction in Carbon Alloy
17 Cathode Catalysts for Polymer Electrolyte Fuel Cells. *J. Power Sources* 2009, **187** (1), 93-97.
- 18 77. Kim, H.; Lee, K.; Woo, S. I.; Jung, Y., On the Mechanism of Enhanced Oxygen Reduction
19 Reaction in Nitrogen-Doped Graphene Nanoribbons. *Phys. Chem. Chem. Phys.* 2011, **13** (39),
20 17505-17510.
- 21 78. Man, I. C.; Su, H. Y.; Calle - Vallejo, F.; Hansen, H. A.; Martínez, J. I.; Inoglu, N. G.; Kitchin, J.;
22 Jaramillo, T. F.; Nørskov, J. K.; Rossmeisl, J., Universality in Oxygen Evolution Electrocatalysis on
23 Oxide Surfaces. *ChemCatChem* 2011, **3** (7), 1159-1165.
- 24 79. McAllister, M. J.; Li, J.-L.; Adamson, D. H.; Schniepp, H. C.; Abdala, A. A.; Liu, J.; Herrera-
25 Alonso, M.; Milius, D. L.; Car, R.; Prud'homme, R. K., Single Sheet Functionalized Graphene by
26 Oxidation and Thermal Expansion of Graphite. *Chem. Mater.* 2007, **19** (18), 4396-4404.
- 27 80. Hutchison, J. E., Greener Nanoscience: A Proactive Approach to Advancing Applications and
28 Reducing Implications of Nanotechnology. *ACS Nano* 2008, **2** (3), 395-402.
29
30
31
32
33
34
35
36
37
38
39
40
41
42
43
44
45
46
47
48
49
50
51
52
53
54
55
56
57
58
59
60

FIGURES AND TABLES

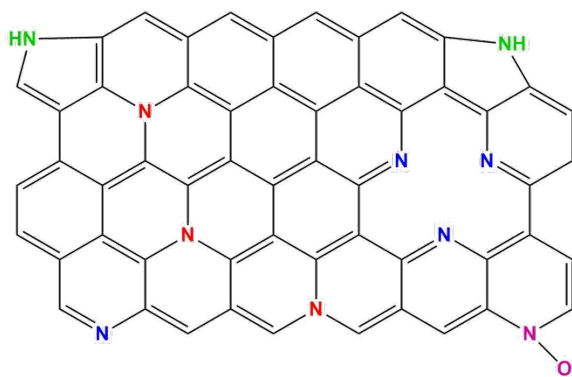


Figure 1. Schematic N-doping configurations in N-doped graphene, including pyridinic-N (blue), pyrrolic-N (green), graphitic-N (red), and N-oxide (purple).

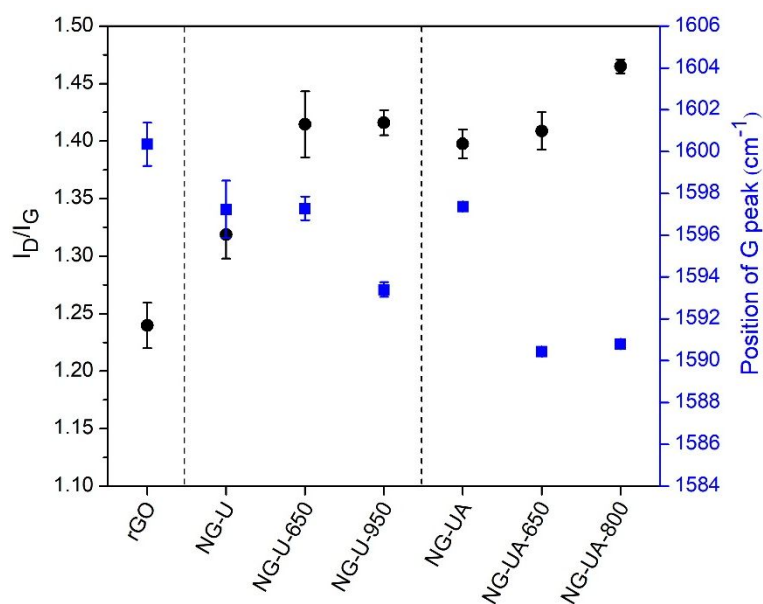


Figure 2. Comparison of the I_D/I_G ratios (black circles, left y-axis) and the position of G peak (blue squares, right y-axis) for rGO and NG samples. The error bars stand for the standard deviation of triplicate measurements in different locations of each sample.

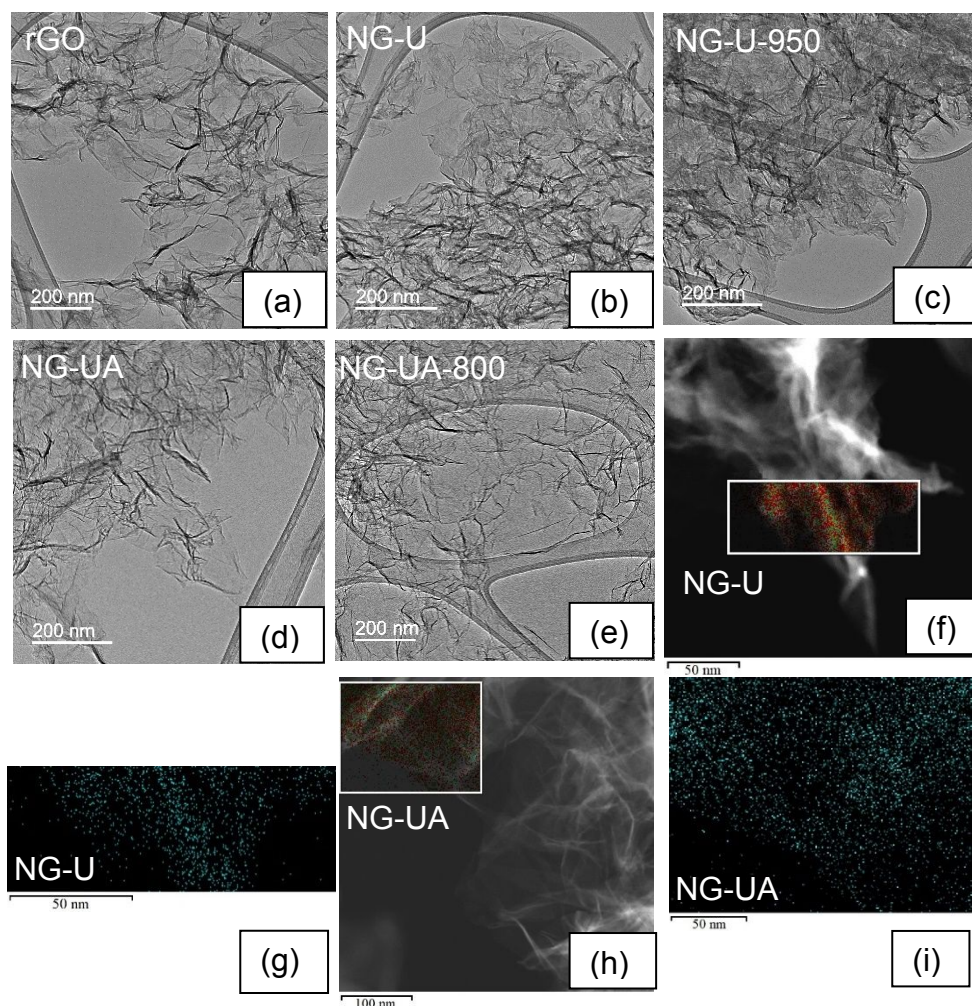


Figure 3. TEM images of rGO (a), NG (b), NG-U-950 (c), NG-UA (d), NG-UA-800 (e), and STEM-EDS elemental maps of selected areas (f and h; red dots for C, green dots for O, and cyan dots for N) indicating the distribution of N (g and i, cyan dots) in NG-U and NG-UA, respectively.

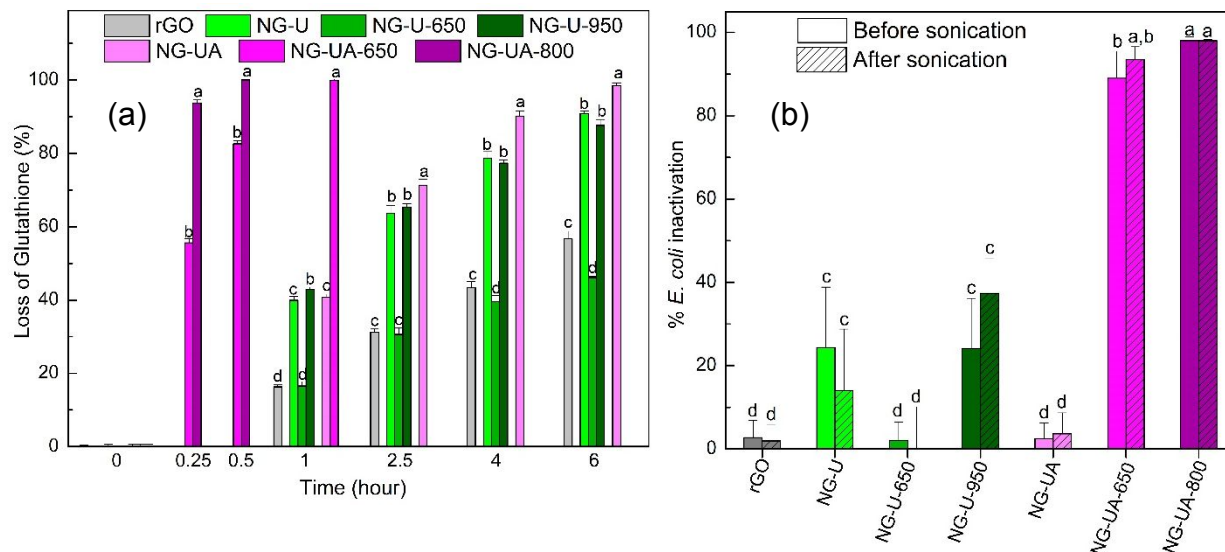


Figure 4. (a) Glutathione (GSH) oxidation by rGO and NG samples for a total 6 h of incubation compared to the control (no rGO/NG). The mass loading of samples is 0.05 mg mL^{-1} and the initial concentration of GSH is 0.4 mM . (b) Cytotoxicity of rGO and NG samples to *E. coli* K12 after 4 h of reaction to 0.2 mg mL^{-1} sample before and after 10 min bath sonication to release viable bacteria wrapped in aggregated graphene sheets. The data were normalized to the control (saline solution without rGO/NG), the cell concentration of the control remained constant after the 4 h incubation and after the 10 min sonication. Means suffixed with different letters (a-d) for each time point are significantly different from each other at $P < 0.05$. Error bars denote the standard deviations of sample replicates.

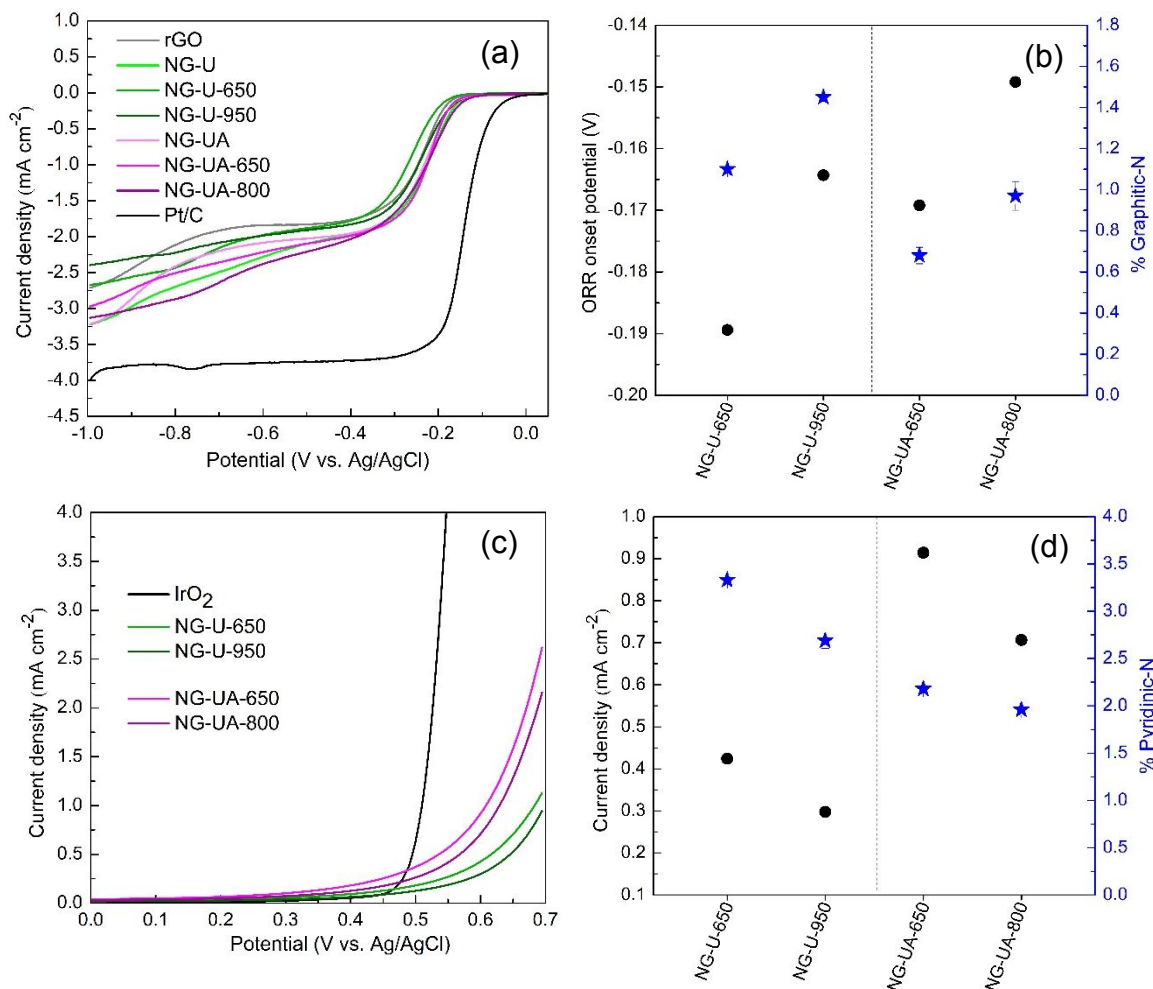


Figure 5. (a) ORR polarization curves of rGO, NG samples, and Pt/C on RRDE in O₂ saturated 1 M KOH with a rotation rate of 1600 rpm and a scan rate of 5 mV s⁻¹. (b) The correlation between the ORR performance of NG (represented by the onset potential) and the percent of graphitic-N (determined by XPS). (c) OER polarization curves of annealed NG samples and IrO₂ on RDE in O₂ saturated 1 M KOH with a rotation rate of 1600 rpm and a scan rate of 5 mV s⁻¹. (d) The correlation between the OER performance of annealed NG samples (represented by the current density at a potential of 0.6 V) and the percent of pyridinic-N (determined by XPS).

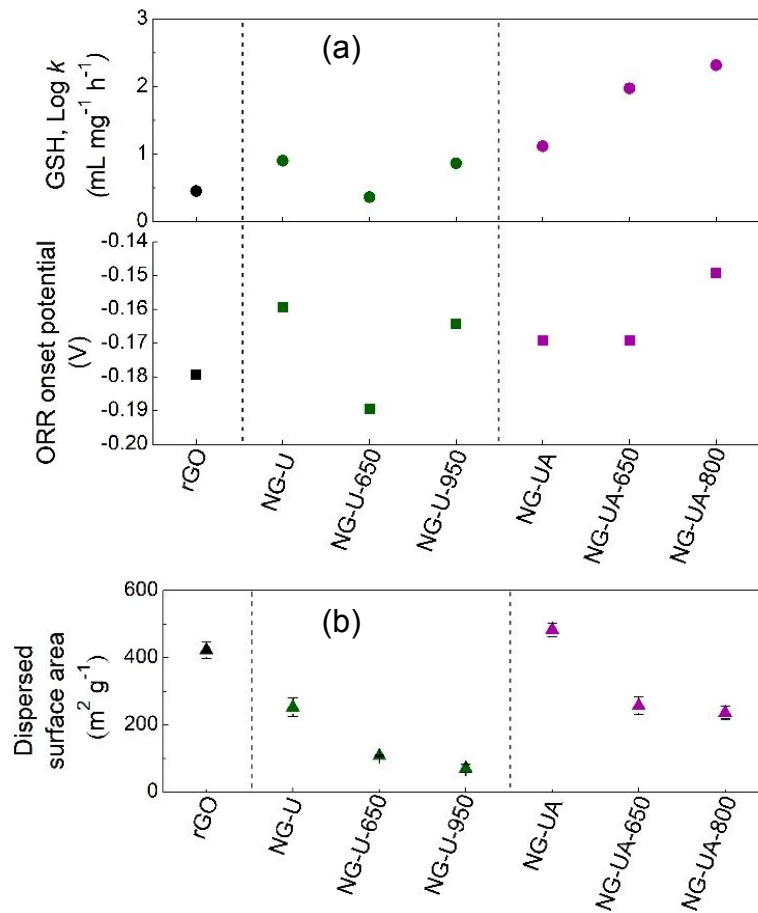


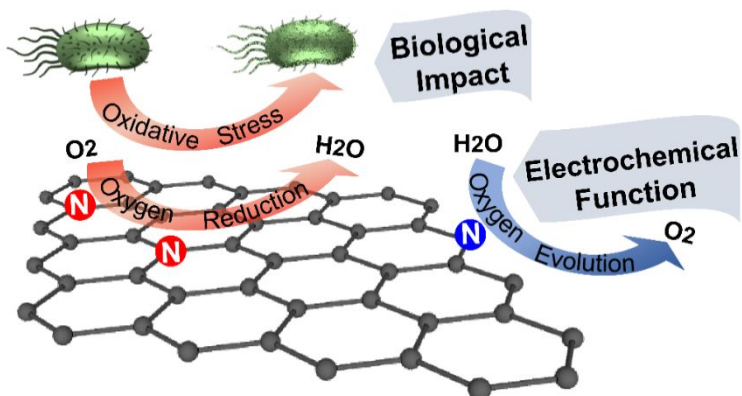
Figure 6. (a) The correlated trends between the rate constants for GSH oxidation and the onset potentials for the ORR activity. (b) The dispersed surface areas in suspension determined by the adsorption of methylene blue (MB).

Table 1. Surface chemistry characterization data for N-doped graphene samples attained from XPS spectra, including the atomic percentage of C, O, and N. The atomic percentage of four predominant nitrogen configurations (pyridinic-N, pyrrolic-N, graphitic-N, and N-oxide) are identified from peak deconvolution of the N1s envelope. The values in the parentheses refer to the percentage distribution of four N-types.

Samples	Annealing Temp. (°C)	% C	% O	% N	Pyridinic-N (% total N)	Pyrrolic-N (% total N)	Graphitic-N (% total N)	N-oxide (% total N)
rGO	/	84.97 ±0.46	15.03 ±0.46	/	/	/	/	/
NG-U	/	82.26 ±0.45	8.57 ±0.08	9.17 ±0.38	2.83±0.06 (30.88%)	4.66±0.11 (50.79%)	0.93±0.01 (10.16%)	0.75±0.04 (8.17%)
NG-U-650	650	88.10 ±0.10	4.88 ±0.06	7.01 ±0.05	3.33±0.04 (47.49%)	2.06±0.04 (29.33%)	1.10±0.01 (15.67%)	0.53±0.01 (7.51%)
NG-U-950	900	90.58 ±0.41	3.72 ±0.35	5.70 ±0.26	2.69±0.08 (47.18%)	1.02±0.07 (17.90%)	1.45±0.02 (25.45%)	0.54±0.05 (9.46%)
NG-UA	/	81.12 ±0.83	12.02 ±0.35	6.86 ±0.48	1.01±0.05 (14.73%)	4.97±0.06 (72.50%)	0.65±0.01 (9.47%)	0.23±0.03 (3.29%)
NG-UA-650	650	91.13 ±0.42	4.63 ±0.44	4.24 ±0.05	2.18±0.03 (51.50%)	1.04±0.03 (24.59%)	0.68±0.04 (15.93%)	0.34±0.02 (7.97%)
NG-UA-800	800	92.98 ±0.23	3.18 ±0.15	3.84 ±0.15	1.96±0.06 (51.10%)	0.54±0.06 (14.11%)	0.97±0.07 (25.20%)	0.37±0.03 (9.58%)

(rGO= the reduced GO after one-step hydrothermal reduction without the addition of nitrogen precursors, serving as the control for NG-U and NG-UA samples; NG-U = N-doped rGO after one-step hydrothermal reduction with urea as the N precursor; NG-UA = N-doped rGO after one-step hydrothermal reduction with uric acid as the N precursor; NG-U-##0 or NG-UA-##0 = thermally annealed NG-U or NG-UA with the maximum temperature indicated by ##0)

TABLE OF CONTENTS ENTRY



Electrochemical techniques are leveraged to probe the influence of N-bonding types on the bioactivity of nitrogen-doped graphene, with graphitic-N identified to be the active site for oxidative stress-related bioactivity.